

11-2014

# Small Carbon Chains in Circumstellar Envelopes

R. J. Hargreaves  
*Old Dominion University*

K. Hinkle

P. F. Bernath  
*Old Dominion University*, [pbernath@odu.edu](mailto:pbernath@odu.edu)

Follow this and additional works at: [https://digitalcommons.odu.edu/chemistry\\_fac\\_pubs](https://digitalcommons.odu.edu/chemistry_fac_pubs)

 Part of the [Astrophysics and Astronomy Commons](#), and the [Chemistry Commons](#)

---

## Repository Citation

Hargreaves, R. J.; Hinkle, K.; and Bernath, P. F., "Small Carbon Chains in Circumstellar Envelopes" (2014). *Chemistry & Biochemistry Faculty Publications*. 71.  
[https://digitalcommons.odu.edu/chemistry\\_fac\\_pubs/71](https://digitalcommons.odu.edu/chemistry_fac_pubs/71)

## Original Publication Citation

Hargreaves, R. J., Hinkle, K., & Bernath, P. F. (2014). Small carbon chains in circumstellar envelopes. *Monthly Notices of the Royal Astronomical Society*, 444(4), 3721-3728. doi:10.1093/mnras/stu1719

# Small carbon chains in circumstellar envelopes

R. J. Hargreaves,<sup>1</sup>★ K. Hinkle<sup>2</sup> and P. F. Bernath<sup>1,3</sup>

<sup>1</sup>Department of Chemistry, Old Dominion University, 4541 Hampton Boulevard, Norfolk, VA 23529, USA

<sup>2</sup>NOAO, 950 North Cherry Avenue, Tucson, AZ 85719, USA

<sup>3</sup>Department of Chemistry, University of York, Heslington, York YO10 5DD, UK

Accepted 2014 August 19. Received 2014 August 15; in original form 2014 July 10

## ABSTRACT

Observations of carbon-rich circumstellar envelopes were made using the Phoenix spectrograph on the Gemini South telescope to determine the abundance of small carbon chain molecules. Vibration–rotation lines of the  $\nu_3$  antisymmetric stretch of  $C_3$  near  $2040\text{ cm}^{-1}$  ( $4.902\text{ }\mu\text{m}$ ) have been used to determine the column density for four carbon-rich circumstellar envelopes: CRL 865, CRL 1922, CRL 2023 and IRC +10216. We additionally calculate the column density of  $C_5$  for IRC +10216, and provide an upper limit for five more objects. An upper limit estimate for the  $C_7$  column density is also provided for IRC+10216. A comparison of these column densities suggests a revision to current circumstellar chemical models may be needed.

**Key words:** astrochemistry – molecular data – stars: abundances – stars: carbon – circumstellar matter – infrared: stars.

## 1 INTRODUCTION

Obscured carbon stars provide us with fascinating environments to study the spectacular mass-loss stage in the evolution of a typical star. In the standard model, stellar pulsation coupled with circumstellar wind ejects mass from the stellar surface into the interstellar medium. The primary consequence of stellar mass-loss is the formation of a circumstellar envelope and during this process the ejected material undergoes several stages of chemical and physical processing (Olofsson 2008). The circumstellar material is made up of molecular gas and ‘dusty’ grains that can provide surfaces for additional processing and grain growth. As the circumstellar shell expands, photochemical processes also become important in the breakdown and formation of further molecules (Ziurys 2006).

It is well established that the carbon to oxygen ( $C/O$ ) ratio dictates the molecular species in circumstellar shells due to the high stability of the CO molecule (Tsuji 1973). This allows a broad variety of molecular species to form from the remaining oxygen-rich or carbon-rich material in circumstellar shells of asymptotic giant branch (AGB) stars (Olofsson 2008). IRC +10216 (CRL 1381) is carbon rich and is the best studied example of a circumstellar shell (Glassgold 1996; Cernicharo et al. 2010; Menten et al. 2012) with more than 80 molecules detected so far, typically from pure rotational spectra (Agúndez et al. 2012). Approximately 80 per cent of these molecules are carbon containing species (Ziurys 2006), although an interesting oxygen chemistry has also been shown to exist (Agúndez & Cernicharo 2006), thus making circumstellar shells a challenging environment for physical and chemical models (Cherchneff 2012).

The smallest pure carbon chains ( $C_2$  and  $C_3$ ) are ubiquitous throughout the interstellar medium (Ádámkóvics, Blake & McCall 2003) and have been detected in diffuse interstellar clouds (Souza & Lutz 1977; Cernicharo, Goicoechea & Caux 2000), comets (Ehrenfreund & Charnley 2000) and star-forming cores (Mookerjee et al. 2012). Pure carbon chains do not possess a permanent dipole moment and therefore do not have allowed pure rotational transitions. A thick ‘dusty’ circumstellar shroud means there is little flux in the visible region and absorptions from electronic transitions cannot be observed due to scattering. However, this makes circumstellar envelopes ideal for observing vibration–rotation bands or low-lying electronic transitions in the infrared. The  $C_2$  (Crampton, Cowley & Humphreys 1975),  $C_3$  (Hinkle, Keady & Bernath 1988) and  $C_5$  (Bernath, Hinkle & Keady 1989) pure carbon chains have been detected in IRC +10216. Longer pure carbon chains have yet to be identified but their derivatives, such as  $HC_n$  ( $n = 1–8$ ),  $H_2C_n$  ( $n = 2–4$ ) and  $HC_{2n}N$  ( $n = 1–5$ ) are prominent species in circumstellar shells and interstellar clouds (Ehrenfreund & Charnley 2000). Small carbon chains ( $C_n$ ) are therefore believed to be the fundamental building blocks of larger carbon containing species, such as polycyclic aromatic hydrocarbons (PAHs), cyanopolynes and fullerenes (Ehrenfreund & Charnley 2000; Kaiser 2002). Indeed, the pure carbon molecules,  $C_{60}$  and  $C_{70}$ , have been observed in planetary nebulae (Cami et al. 2010). Small carbon chains are also important in flame chemistry (Baronovski & McDonald 1977) and soot formation (Goulay et al. 2010).

Understanding circumstellar chemistry relies heavily on the archetypical object IRC +10216 due to its proximity and large mass-loss (Olofsson 2008; Agúndez et al. 2012). Spectral surveys have been performed on circumstellar shells around other carbon stars, such as CIT 6 (Zhang, Kwok & Dinh-V-Trung 2009a) and CRL 3068 (Zhang, Kwok & Nakashima 2009b), which both show a

★E-mail: rhargrea@odu.edu

**Table 1.** Observations using the Phoenix spectrometer on Gemini South (GS-2010A-Q-74).

Object	IRAS	Magnitude			Observation dates in 2010 (integration time in minutes)			Magnitude references
		<i>J</i>	<i>H</i>	<i>K</i>	<i>C</i> <sub>3</sub> region	<i>C</i> <sub>5</sub> region	<i>C</i> <sub>7</sub> region	
<i>Programme stars:</i>								
CRL 865	06012+0726	–	11.3	7.7	24 Feb (24)	21 Feb (16)	23 Feb (32)	1
IRC +10216	09452+1330	7.3	4.0	1.2	03 Mar (0.8)	25 Feb (5.3)	23 Feb (8)	1
CRL 1922	17049–2440	12.2	9.2	6.3	12 Jun (8)	01 Mar (8)	26 Apr (16)	2
CRL 2023	17512–2548	13.2	9.5	6.5	12 Jun (16)	04 Mar (38)	22 May (32)	2
CRL 2178	18288–0837	11.7	8.0	5.2	–	23 May (52)	27 Jun (21.3)	2
CRL 3099	23257+1038	–	10.3	7.1	–	27 Jun (24)	–	1
<i>Reference stars:</i>								
HIP 22509	04478 + 0848	4.26	4.21	4.17	–	21 Feb (16)	–	3, 4
HR 1790	05224 + 0618	2.17	2.24	2.32	24 Feb (38)	–	–	3
HR 2491	06429 – 1639	–1.36	–1.33	–1.35	–	25 Feb (2.7)	23 Feb (1.3)	3
HR 4662	12132 – 1715	2.76	2.83	2.81	12 Jun (50)	–	–	3
HR 5267	14002 – 6008	1.17	1.21	1.28	03 Mar (96)	01 Mar (48)	27 Jun (48)	4
HR 6553	17337 – 4258	1.07	0.87	0.84	–	04 Mar (24) 23 May (40) 27 Jun (53.3)	26 Apr (40) 22 May (40)	4

*References.* (1) Whitelock et al. (2006); (2) Chen & Yang (2012); (3) Ducati (2002); (4) Cutri et al. (2003).

similar chemical composition to IRC +10216. However, as a carbon-rich AGB star evolves, the chemical composition changes primarily due to photochemical processes (Cernicharo, Agúndez & Guélin 2011). The circumstellar winds transport molecules and dust into the envelope where chemical pathways are thought to lead to the formation of carbon chains and aromatic rings (Cherchneff 2006, 2012). These molecules are then broken down as a part of the AGB shell evolution towards planetary nebulae. Determining the abundance of small chains in circumstellar shells allow chemical models to be refined, whilst comparing carbon chain abundances between carbon-rich circumstellar shells determines the appropriateness of IRC +10216 as the prototypical example.

Vibration–rotation transitions of pure carbon chains allow the detection of these molecules in circumstellar envelopes when high-resolution experimental data are available. The  $\nu_3$  antisymmetric stretch of  $C_3$  has been the focus of a number of experimental and theoretical studies (Matsumura et al. 1988; Moazzen-Ahmadi & McKellar 1993; Špirko, Mengel & Jensen 1997), and has a band centre at  $2040.019\text{ cm}^{-1}$  (vacuum wavelength<sup>1</sup>  $4.901\,915\text{ }\mu\text{m}$ ; Krieg et al. 2013). The  $\nu_3$  mode of  $C_3$  has also been investigated (Moazzen-Ahmadi, McKellar & Amano 1989; Vala et al. 1989; Massó et al. 2007) with a band centre at  $2169.442\text{ cm}^{-1}$  ( $4.609\,480\text{ }\mu\text{m}$ ; Bernath et al. 1989).  $C_7$  has yet to be detected in circumstellar envelopes, but the strongest vibrational band, the  $\nu_4$  antisymmetric stretch at  $2138.314\text{ cm}^{-1}$  ( $4.676\,582\text{ }\mu\text{m}$ ; Neubauer-Guenther et al. 2007), has been measured in the laboratory (Heath & Saykally 1991; Mogren Al-Mogren, Senent & Hochlaf 2013). The close proximity of these fundamental frequencies (within  $0.3\text{ }\mu\text{m}$ ) allow all three molecules to be studied in circumstellar shells using the same high-resolution instrument.

## 2 OBJECTS AND OBSERVATIONS

High-resolution infrared spectra were obtained of target carbon stars with known circumstellar shells using the 8.1 m Gemini South tele-

scope and the NOAO Phoenix spectrometer (Hinkle et al. 1998). The observations (GS-2010A-Q-74) were carried out during the first half of 2010 and the programme stars are listed in Table 1. All programme stars are tip AGB Mira variables and their  $K$ -band flux varies by approximately one magnitude. In addition to the programme stars, a number of hotter reference stars were also observed for the removal of telluric features.

The Phoenix spectrometer is a cryogenically cooled echelle spectrograph that uses order-separating filters to isolate individual echelle orders. The detector is a  $1024 \times 1024$  InSb Aladdin II array. A 2 pixel slit width was used resulting in a spectral resolving power of  $R = \lambda/\Delta\lambda \sim 70\,000$ . Three spectral regions were observed centred on  $2045\text{ cm}^{-1}$  ( $4.890\text{ }\mu\text{m}$ ),  $2168\text{ cm}^{-1}$  ( $4.613\text{ }\mu\text{m}$ ) and  $2138\text{ cm}^{-1}$  ( $4.677\text{ }\mu\text{m}$ ) to cover the corresponding  $C_3$ ,  $C_5$  and  $C_7$  vibration bands. The size of the detector along the dispersion direction limits the wavelength coverage for a single observation to  $\sim 0.5$  per cent (e.g., a dispersion of  $\sim 10.5\text{ cm}^{-1}$  at  $2100\text{ cm}^{-1}$ ).

The observations and reductions employed standard thermal infrared techniques (Joyce 1992) and used the IRAF software package.<sup>2</sup> The spectra were wavelength calibrated using telluric lines of CO from HITRAN (Rothman et al. 2013) and a typical rms uncertainty in the wavenumber scale is less than  $0.005\text{ cm}^{-1}$ . The same HITRAN lines were used in the calculation of the telluric model atmospheres (see Section 3).

## 3 MODEL ATMOSPHERES AND TELLURIC REMOVAL

The reference star observations, listed in Table 1, consistently have a lower signal-to-noise compared to the object spectra for which the typical signal-to-noise ratio is  $\sim 500$ . When the reference spectra are used to correct for atmospheric absorption, the object spectra are degraded. Recently, Seifahrt et al. (2010) have demonstrated

<sup>1</sup> All wavelengths are given for vacuum.

<sup>2</sup> IRAF software is distributed by the National Optical Astronomy Observatories under contract with the National Science Foundation.

the advantage of using synthetically produced absorption atmospheric spectra to remove telluric features from spectra taken with the CRILES spectrograph.

The Reference Forward Model<sup>3</sup> (RFM) is a line-by-line radiative transfer model used to calculate atmospheric transmission spectra and is often used to interpret satellite observations (Fischer et al. 2008). RFM can be used to compute the atmospheric transmission for an observer at any zenith angle, making RFM well suited to simulating astronomical reference spectra for telescope observations with differing airmass. The primary advantage of using RFM in place of the observed reference spectra is to eradicate noise introduced during the removal of telluric lines.

The synthetic spectra computed for this study were calculated using RFM v4.30, which uses the HITRAN 2012 data base for molecular line parameters (Rothman et al. 2013). The Michelson Interferometer for Passive Atmospheric Sounding (MIPAS) night time model atmospheric profiles (*ngt.atm*) were used with the CO<sub>2</sub> profile scaled to 2010 concentrations and the H<sub>2</sub>O profile scaled to match observation. A Gaussian instrument lineshape (FWHM = 0.03 cm<sup>-1</sup>) was also used to account for the lineshape of the Phoenix spectrometer. In addition, telescope temperature measurements were combined with National Centers for Environmental Prediction temperature profiles for Gemini South during the period of measurement to adjust the temperature profile below 25 km (i.e. the troposphere and lower stratosphere). Above 25 km, the MIPAS *ngt.atm* temperature profile remained unchanged. Since the H<sub>2</sub>O absorptions and weather conditions were different for each observation, it was necessary to produce an RFM synthetic spectrum for each programme observation to replace the reference star observations.

The IRAF routine TELLURIC was used to remove telluric features and to ratio programme stars with the RFM synthetic spectra. Fig. 1 shows the observed C<sub>3</sub> spectral region (approximately 2041–2049 cm<sup>-1</sup>) for IRC +10216 and the corresponding RFM synthetic spectrum, with strongly absorbing telluric features indicated. The resulting spectrum for IRC +10216 is also shown in Fig. 1 with circumstellar molecular lines identified. Whilst complete removal of some telluric features is not achieved (e.g. H<sub>2</sub>O and CO<sub>2</sub>), the result is an improvement on telluric removal when the reference star spectra are used. The C<sub>3</sub> absorptions are sharp and of moderate intensity (~15 per cent absorption) and can be identified before telluric features have been removed. The CO lines are unlike C<sub>3</sub> because they have characteristic P-Cygni profiles due to the distribution of CO throughout the circumstellar envelope at different radial velocities (Keady, Hall & Ridgway 1988).

## 4 RESULTS

### 4.1 C<sub>3</sub>

Telluric removal was carried out on all observations from Table 1 using RFM synthetic spectra. The observed C<sub>3</sub> spectral region contained the R(2), R(4), R(6) and R(8) rotational lines of the ν<sub>3</sub> anti-symmetric stretch at 2042.66, 2044.48, 2046.32 and 2048.20 cm<sup>-1</sup>, respectively. Table 2 summarises the line identifications for each of the programme stars. Missing R-branch lines are due to absorption coincidences with telluric features due to relative velocity shifts.

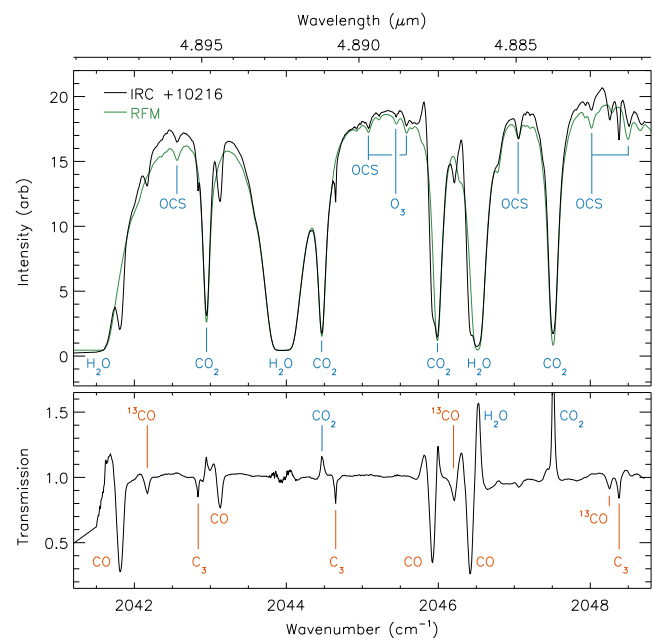


**Figure 1.** Calibrated spectrum of IRC +10216 with the corresponding RFM synthetic spectrum (upper panel) and resulting ratioed IRC +10216 spectrum with telluric lines removed (lower panel). Molecular absorption from telluric lines (blue) and the circumstellar shell (orange) have been indicated.

From these observations, the column densities and local standard of rest velocity shifts were calculated.

The ratioed programme star spectra were normalized and the baseline was flattened to account for small variations over the observed region. The C<sub>3</sub> absorption peaks were fit to a Gaussian lineshape using ORIGINPRO 8.0. The rotational temperature of C<sub>3</sub> within the circumstellar envelope can be calculated from the relationship between the absorption intensity  $I$ , to temperature  $T$  (Herzberg 1989), since

$$I \propto (J' + J'' + 1)e^{-B''J''(J''+1)hc/kT}, \quad (1)$$

where  $B'' = 0.436$  cm<sup>-1</sup> (Krieg et al. 2013). The slope obtained from  $\ln[I/(J' + J'' + 1)]$  versus  $J''(J'' + 1)$  yields  $-B''hc/kT$  and thus the temperature. The C<sub>3</sub> temperature for each programme star is given in Table 2 based on the identification of each C<sub>3</sub> peak. For CRL 2023, only two lines were observed (giving a rotational temperature of 133 K) therefore an estimated temperature of 50 K was used instead.

The molecular C<sub>3</sub> column densities can be obtained from the Beer–Lambert law

$$I = I_0 e^{-S'g(v-v_{10})NI}, \quad (2)$$

where  $S'$  is the ‘line strength’,  $I$  is the line intensity and  $g(v - v_{10})$  is the line shape function (Bernath 2005). Integrating over the whole line and rearranging for column density  $NI$  gives

$$NI = \frac{1}{S'} \int \ln(I_0/I) dv, \quad (3)$$

where the integral is given by the area of each C<sub>3</sub> absorption peak and line strength,  $S'$ , is obtained from

$$S' = \frac{2\pi^2\nu_{10}S_{J'J''}}{3\epsilon_0hcQ} e^{-E_0/kT} (1 - e^{h\nu/kT}). \quad (4)$$

The partition functions  $Q$ , was calculated individually for each programme star (Table 2) based on the temperature and the

<sup>3</sup> Reference Forward Model, RFM (v4.30), A. Dudhia, University of Oxford, <http://www.atm.ox.ac.uk/RFM>.

**Table 2.** Summary of C<sub>3</sub> line identifications.

Programme star	Observed lines <sup>a</sup> (cm <sup>-1</sup> )				Obs-Ref <sup>b</sup> (cm <sup>-1</sup> )	Temperature (K)	Partition function	Column density (cm <sup>-2</sup> )
	R(2)	R(4)	R(6)	R(8)				
CRL 865	2042.188	–	2045.845	2047.718	–0.480	44.3	40.3	$9.6 \times 10^{14}$
IRC +10216	2042.835	2044.647	–	2048.377	+0.172	49.1	46.9	$8.8 \times 10^{14}$
CRL 1922	2042.888	2044.670	–	2048.423	+0.222	29.3	24.8	$6.8 \times 10^{14}$
CRL 2023	–	2044.714	–	2048.432	+0.233	50.0 <sup>c</sup>	57.4	$3.8 \times 10^{14}$

<sup>a</sup>In telluric frame of reference.<sup>b</sup>Average observed–reference (references determined from Krieg et al. 2013).<sup>c</sup>Estimated temperature.

contribution due to the rotational and vibrational components. The rotational line strength,  $S_{J'J''}$ , was calculated from the transition dipole moment  $M_{v'v''}$  (Bernath 2005) as

$$S_{J'J''} = |M_{v'v''}|^2 \text{HLF}, \quad (5)$$

where HLF is the Hönl–London Factor ( $\text{HLF} = J'' + 1$  for *R*-branch lines of C<sub>3</sub>) and  $M_{v'v''} = 0.35$  debye (Jensen, Rohlfing & Almloef 1992).

The spectral simulation program PGOPHER<sup>4</sup> was used to simulate the rotational spectrum of the  $\nu_3$  band of C<sub>3</sub> using the calculated temperature with the constants from Krieg et al. (2013). This provided the lower state energy,  $E_0$ , for each transition along with the rotational assignments.

From equation (3), the average column densities of C<sub>3</sub> are calculated to be  $9.6 \times 10^{14}$ ,  $8.8 \times 10^{14}$ ,  $6.8 \times 10^{14}$  and  $3.8 \times 10^{14}$  cm<sup>-2</sup> for CRL 865, IRC +10216, CRL 1922 and CRL 2023, respectively. These calculated column densities have an estimated error of 20 per cent except CRL 2023, which is about a factor of 2 due to the estimated temperature. Fig. 2 displays the *R*(8) line of the  $\nu_3$  mode of C<sub>3</sub> for the programme stars given in Table 2. The fitted Gaussian peak is displayed along with the area used to calculate the C<sub>3</sub> column density.

The sharp line shape of C<sub>3</sub> indicates that the molecule is contained within a narrow shell of each circumstellar envelope. Calibrating the spectra with telluric features determines the velocity shift ( $v_{\text{obs}}$ ) of the observed line. The IRAF procedure RVCORRECT was used to calculate the velocity shifts due to the motion of the Earth, Moon and Sun at the time of observation to provide the local standard of rest velocity ( $v_{\text{lsr}}$ ). Comparing the  $v_{\text{lsr}}$  values to accepted stellar velocities ( $v_{\text{obs}}$ ) for each object, the shell expansion velocity ( $v_{\text{shell}}$ ) can be obtained from  $v_{\text{shell}} = v_{\text{lsr}} - v_{\text{obj}}$ ; the results are summarized in Table 3.

#### 4.2 C<sub>5</sub>

A PGOPHER simulation of the  $\nu_3$  mode of C<sub>5</sub> at 50 K using the constants obtained from Moazzen-Ahmadi et al. (1989) and a band strength of 0.74 debye (Botschwina & Sebald 1989) predicts the *P*(14) transition to be the most intense. Fig. 3 displays the velocity shifted and ratioed spectrum for IRC +10216 in the proximity of the *P*(14) transition, a number of small absorption features are coincident to the C<sub>5</sub> positions. There are tentative identifications of the *P*(8), *P*(10), *P*(16) and *P*(20) lines; the remaining lines are contaminated by telluric features and cannot be identified. The column density calculated from the strongest transition, *P*(8), is

<sup>4</sup>PGOPHER (v8.0.195), a program for simulating rotational structure, C. M. Western, University of Bristol, <http://pgopher.chm.bris.ac.uk/>.

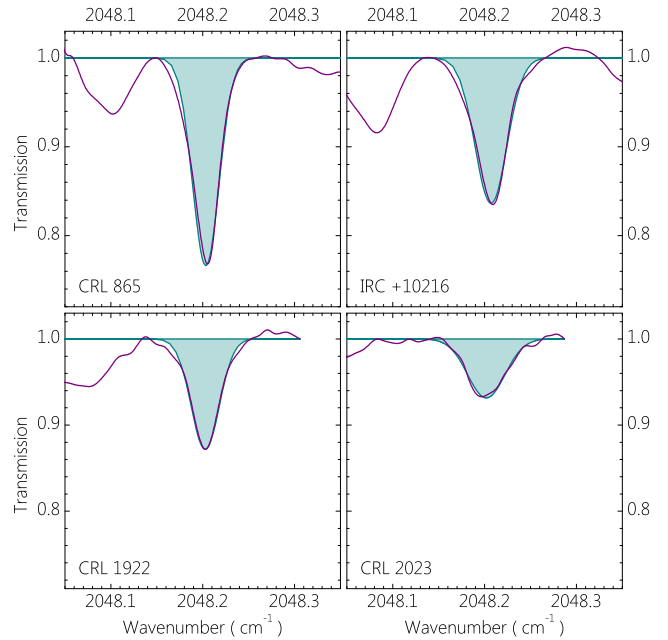


**Figure 2.** Calibrated identification of the *R*(8) absorption line of the  $\nu_3$  mode of C<sub>3</sub> at 2048.2 cm<sup>-1</sup> (4.882  $\mu$ m) for observations in the circumstellar shells of CRL 865, IRC +10216, CRL 1922 and CRL 2023. The shaded region indicates the fitted area used to calculate the column density for each line.

$1.3 \times 10^{13}$  cm<sup>-2</sup>. This calculation has been carried out for the *P*(8) transition in the spectra of the remaining objects observed in the C<sub>5</sub> region. These features are not as prominent as they are in IRC +10216 and the calculated column densities are estimated upper limits as summarized in Table 4.

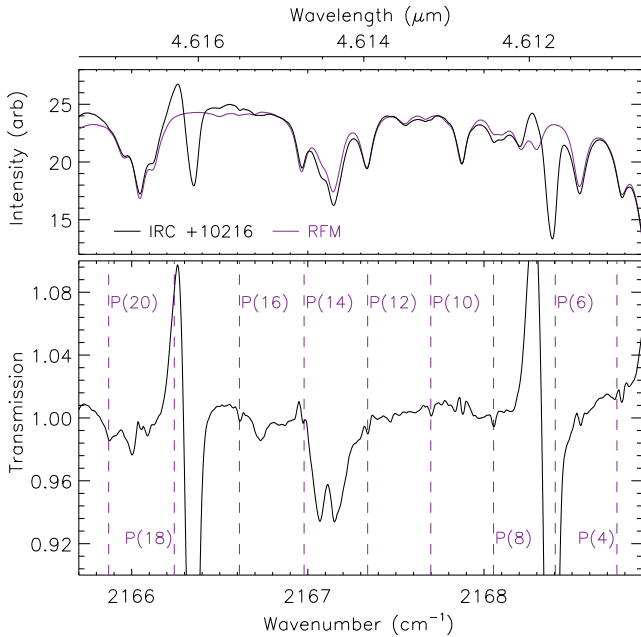
#### 4.3 C<sub>7</sub>

A PGOPHER simulation of the  $\nu_4$  mode of C<sub>7</sub> at 50 K using the constants obtained from Neubauer-Guenther et al. (2007) and a band strength of 0.72 debye determined from a band intensity of 2809 km mol<sup>-1</sup> (Kranze, Rittby & Graham 1996) predicts the *R*(24) transition to be the most intense. Fig. 4 displays the reduced spectrum for IRC +10216 with predicted C<sub>7</sub> line positions. No assignments can be made above the noise limit. The small ‘peak’ at 2140.12 cm<sup>-1</sup> near *R*(30) has been used to estimate an upper limit of the C<sub>7</sub> column density, assuming the molecule is contained within a shell at 50 K. The calculated upper limit for the C<sub>7</sub> column density in the circumstellar envelope of IRC +10216 is  $4.7 \times 10^{12}$  cm<sup>-2</sup>.

**Table 3.** Velocity components (in  $\text{km s}^{-1}$ ) for each programme star from the velocity shifted  $\text{C}_3$  absorptions.

Object	Observed velocity ( $v_{\text{obs}}$ )	Local standard of velocity ( $v_{\text{lsr}}$ )	Stellar Rest velocity <sup>a</sup> ( $v_{\text{obj}}$ )	Shell velocity ( $v_{\text{shell}}$ )
CRL 865	70.3	28.5	45.6	-17.1
IRC +10216	-25.2	-41.1	-23.2 (-26.0 <sup>b</sup> )	-17.9 (-15.1)
CRL 1922	-32.6	-22.6	-5.1	-17.5
CRL 2023	-34.1	-18.7	-	-18.7

<sup>a</sup> From Menzies, Feast & Whitlock (2006).

<sup>b</sup> From Menten et al. (2012).

**Figure 3.** A section of the calibrated and velocity shifted spectrum of IRC +10216 and the corresponding RFM synthetic spectrum in the range of the  $\nu_3$  mode of  $\text{C}_5$  (upper panel). The ratioed IRC +10216 spectrum highlights the position of the  $P$ -branch absorptions shown in purple (lower panel).

**Table 4.** Upper limit estimates for the  $\text{C}_5$  column densities.

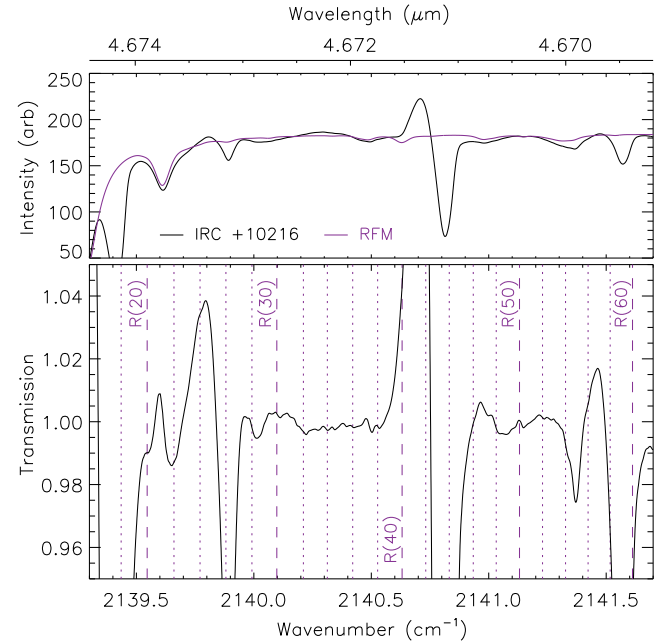
Object	Column density upper limit <sup>a</sup> ( $\text{cm}^{-2}$ )	Ratio <sup>b</sup>
CRL 2023	$2.4 \times 10^{12}$	158
CRL 3099	$5.1 \times 10^{12}$	-
CRL 865	$9.4 \times 10^{12}$	102
CRL 2178	$1.1 \times 10^{13}$	-
CRL 1922	$1.2 \times 10^{13}$	57
IRC +10216	$1.3 \times 10^{13}$	68

<sup>a</sup> Except for IRC +10216.

<sup>b</sup> As  $\text{C}_3:\text{C}_5$  column density.

## 5 DISCUSSION

Synthetic reference spectra were necessary due to the unsatisfactory noisy reference star spectra, which in some cases had noise close to 5 per cent. We have demonstrated that line-by-line radiative transfer programs, such as RFM, are capable of creating suitable reference spectra for the removal of telluric features from obscured carbon


**Figure 4.** A section of the calibrated and velocity shifted spectrum of IRC +10216 and the corresponding RFM synthetic spectrum in the range of the  $\nu_4$  mode of  $\text{C}_7$  (top panel). The  $R$ -branch line positions are shown in purple along with the ratioed IRC +10216 spectrum (lower panel).

stars in the infrared. These objects have complicated absorption spectra and a complete removal of telluric features is often difficult. Our synthetic spectra were created using a combination of measured and standard atmospheric conditions for the Gemini observatory. We restricted our adjustment of the standard RFM molecular atmospheric profiles to a scaling of the  $\text{CO}_2$  and  $\text{H}_2\text{O}$  profiles. This kept the remaining molecular profiles consistent and accounts for differing humidity conditions during each observation. We also adjusted the standard temperature profile (which applies to all molecules) to coincide with the measured temperature at the telescope. For these reasons, the synthetic spectra do not completely remove telluric features; however, it should be noted that this was also not possible using the original reference star observations, most likely due to the fluctuating weather conditions during each observation run. Telescope time is a limited resource and is better spent on object acquisition, particularly if synthetic spectra are able to adequately simulate reference star observations.

The  $\text{C}_3$  absorptions are clearly identifiable due to the strength of the  $\nu_3$  transition. They can be assigned before telluric removal (Fig. 1) and were observed in the spectra of all programme stars

**Table 5.** Summary of the observed and calculated column densities (in  $\text{cm}^{-2}$ ) of small carbon chains in IRC +10216.

Carbon chain	This work	Observed (Ref.)	Calculated (Ref.)
C <sub>3</sub>	$8.8 \times 10^{14}$	$1.0 \times 10^{15}$ (1)	$2.0 \times 10^{14}$ (4)
C <sub>5</sub>	$1.3 \times 10^{13}$	$9.0 \times 10^{13}$ (2)	$2.0 \times 10^{14}$ (4)
C <sub>7</sub>	$\leq 4.7 \times 10^{12}$	$\leq 2.0 \times 10^{13}$ (3)	$1.1 \times 10^{14}$ (5)

*References.* (1) Hinkle et al. (1988); (2) Bernath et al. (1989); (3) Hinkle & Bernath (1993); (4) Li et al. (2014); (5) Millar et al. (2000).

recorded in the C<sub>3</sub> region. These absorptions are underresolved at a resolution of  $0.03 \text{ cm}^{-1}$  and the sharp transitions are broadened by the instrument line shape function, resulting in a reduced absorption depth. Nevertheless, the calculated column density of  $8.8 \times 10^{14} \text{ cm}^{-2}$  for C<sub>3</sub> in IRC +10216 compares very well to  $1.0 \times 10^{15} \text{ cm}^{-2}$  obtained by Hinkle et al. (1988).

The same broadening occurs for our C<sub>5</sub> observations and a maximum absorption depth of  $\sim 1$  per cent is seen. It was only possible to calculate the column density of C<sub>5</sub> in IRC +10216 by using a synthetic spectrum to remove the telluric lines. C<sub>5</sub> has previously been observed with a column density of  $9.0 \times 10^{13} \text{ cm}^{-2}$  in the same spectral region of IRC +10216 by Bernath et al. (1989) using a high-resolution Fourier transform infrared spectrometer ( $0.01 \text{ cm}^{-1}$  resolution); a maximum absorption depth of  $\sim 3$  per cent was observed. The calculated value of  $1.3 \times 10^{13} \text{ cm}^{-2}$  is approximately 15 per cent of the value calculated by Bernath et al. (1989); however, Botschwina & Sebald (1989) suggest that the Bernath et al. (1989) column density was an overestimate due to the transition dipole moment that was used. The C<sub>5</sub> transition dipole moment for this study was taken from Botschwina & Sebald (1989) and the column density presented here is within 25 per cent of their estimated value of  $5.0 \times 10^{13} \text{ cm}^{-2}$ .

The C<sub>5</sub> absorption lines for the remaining programme stars (excluding IRC +10216) are at the noise limit when synthetic reference spectra are used. Therefore, it was only possible to provide an estimate of the upper limit for C<sub>5</sub> in these objects. Whilst these upper limits span almost one order of magnitude, and therefore should only be used as an indication, it is interesting to note a negative correlation between the column density of C<sub>5</sub> and the C<sub>3</sub>:C<sub>5</sub> ratio.

Hinkle & Bernath (1993) have previously obtained an upper limit of  $2.0 \times 10^{13} \text{ cm}^{-2}$  for a C<sub>7</sub> column density based on high-resolution spectra of IRC +10216. This work refines the column density upper limit for C<sub>7</sub> in IRC +10216 by almost one order of magnitude to  $4.7 \times 10^{12} \text{ cm}^{-2}$ . The column densities of C<sub>3</sub>, C<sub>5</sub> and C<sub>7</sub> are summarized and compared to previously determined and calculated values for IRC +10216 in Table 5.

The total empirical column density in IRC +10216 for neutral carbon is  $1.1 \times 10^{16} \text{ cm}^{-2}$  (Keene et al. 1993) and for C<sub>2</sub> is  $7.9 \times 10^{14} \text{ cm}^{-2}$  (Bakker et al. 1997). Fig. 5 includes these values with those for C<sub>3</sub>, C<sub>5</sub> and C<sub>7</sub> from this study and compares the empirical column densities to the number of carbon atoms. Also included in Fig. 5 are calculated column densities for all pure carbon species from Millar et al. (2000) and the appropriate values from McElroy et al. (2013). Carbon chain column densities from a state-of-the-art model by Li et al. (2014), that improves the N<sub>2</sub> and CO photodissociation rates and shield functions of McElroy et al. (2013), is also shown.

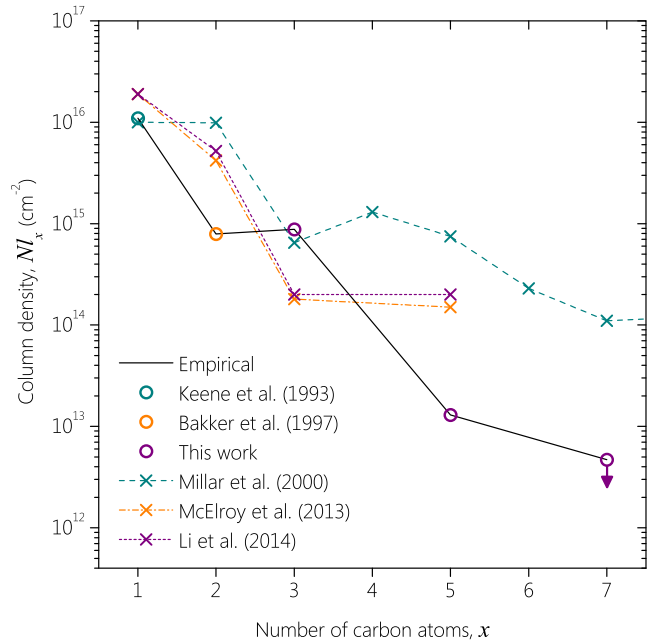
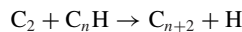
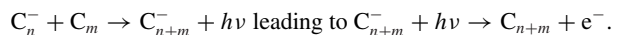


**Figure 5.** A comparison of the column densities of small carbon chain species in IRC +10216. Empirical column densities are shown by the solid black line and include the values for neutral carbon (Keene et al. 1993), C<sub>2</sub> (Bakker et al. 1997) and C<sub>3</sub>, C<sub>5</sub> and C<sub>7</sub> from this work. The dashed lines refer to calculated column densities for IRC +10216 by Millar, Herbst & Bettens (2000), McElroy et al. (2013) and Li et al. (2014).

The primary carbon chains growth pathways (Millar et al. 2000) are given by



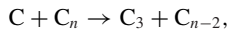
and



The latest models have reduced the column densities of C<sub>3</sub> and C<sub>5</sub>; however, there is still disagreement between observation and calculation. Most notably, C<sub>3</sub> is underestimated whereas C<sub>5</sub> is overestimated. The calculated values from Millar et al. (2000), McElroy et al. (2013) and Li et al. (2014), shown in Fig. 5, predict the column densities of C<sub>3</sub> and C<sub>5</sub> to be almost equal. Our work suggests that C<sub>3</sub> is almost two orders of magnitude greater than C<sub>5</sub> (see Table 5), which indicates a similar trend to that seen in Cherchneff & Glassgold (1993) where the abundance of C<sub>3</sub> was  $\sim 10$  times greater than C<sub>5</sub>. The empirical column densities for small carbon chains (particularly C<sub>2</sub>, C<sub>3</sub> and C<sub>5</sub>) indicate that the reaction rates for small carbon chains in current models are incorrect; the models are missing important reactions; or the choice of initial circumstellar conditions is not suitable.

Carbon containing molecules are ubiquitous throughout the interstellar medium and are not confined to circumstellar envelopes (Herbst & van Dishoeck 2009). Linear carbon chain growth is thought to eventually lead to larger species like PAHs, cyanopolyynes, fullerenes and even amino acids. Benzene (C<sub>6</sub>H<sub>6</sub>) has been detected in proto-planetary nebula (Cernicharo et al. 2001), cyanopolyne species containing a chain of as many as 11 carbon atoms (HC<sub>11</sub>N) have been observed in dark interstellar clouds (Bell et al. 1997) and large fullerenes, such as C<sub>60</sub> and C<sub>70</sub>, have been observed in planetary nebulae (Cami et al. 2010). Loison et al. (2014)

consider a revised chemical model for dark interstellar clouds that includes a number of reactions that break down larger linear carbon chains into smaller chains via reaction pathways such as



where  $n \geq 4$ . They note that the consequence for linear carbon chains is to limit the abundance of longer chains ( $C_{n>3}$ ) due to faster reaction rates, resulting in an accumulation of  $C_3$ , which has an estimated low reactivity. This would have the consequence of increasing the  $C_3$  column density at the expense of  $C_5$  (and longer chains), which would appear to improve current model calculations (Fig. 5).

The  $C_3$  column densities can be used to determine an average column density of  $7.3 \times 10^{14} \text{ cm}^{-2}$  for the circumstellar envelopes of carbon-rich AGB stars. However, not all carbon stars have equivalent C/O ratios or mass-loss rates, which are essential in understanding the circumstellar chemistry. The C/O ratio for IRC +10216 is given as 1.4 and the mass-loss rate has been calculated as  $3.3 \times 10^{-5} M_{\odot} \text{ yr}^{-1}$  (Bergeat & Chevallier 2005), but these parameters are unavailable for the remaining objects so no correlations can be investigated. Since  $C_3$  was observed in all objects, we believe IRC +10216 remains a prototypical example.

Bakker et al. (1997) identified a correlation between  $C_2$  column densities and circumstellar expansion velocity. Our results show no correlation between  $C_3$  or  $C_5$  column densities with the shell velocity; however, if the more recent stellar velocity of  $-26.0 \text{ km s}^{-1}$  (Menten et al. 2012) is used for IRC +10216, a slight increase in column density is seen for decreasing shell velocity. Our velocities are consistent and indicate a typical circumstellar shell velocity to be approximately  $17.5 \text{ km s}^{-1}$ .

## 6 CONCLUSIONS

The small carbon chain  $C_3$  has been detected in the circumstellar envelopes of CRL 865, IRC +10216, CRL 1922 and CRL 2023 by the identification of a number of vibration–rotation lines from the  $\nu_3$  antisymmetric stretch of  $C_3$  near  $2040 \text{ cm}^{-1}$ . The calculated column densities are  $9.6 \times 10^{14}$ ,  $8.8 \times 10^{14}$ ,  $6.8 \times 10^{14}$  and  $3.8 \times 10^{14} \text{ cm}^{-2}$ , respectively. We used synthetic spectra to remove telluric features from our observations, highlighting how a line-by-line radiative transfer model can be used to remove telluric features if reference star spectra are of poor quality or unavailable.  $C_5$  was observed in IRC +10216 with a column density of  $1.3 \times 10^{13} \text{ cm}^{-2}$ , and upper limits have been provided for five for other sources. An upper limit for the column density of  $C_7$  in IRC +10216 was estimated to be  $4.7 \times 10^{12} \text{ cm}^{-2}$ . Our measurements suggest a revision to circumstellar shell models may be needed to account for small carbon chain abundances.

## ACKNOWLEDGEMENTS

This work is based on observations obtained at the Gemini Observatory, which is operated by the Association of Universities for Research in Astronomy, Inc., under cooperative agreement with the NSF on behalf of the Gemini partnership: the National Science Foundation (United States), the National Research Council (Canada), CONICYT (Chile), the Australian Research Council (Australia), Ministério da Ciência, Tecnologia e Inovação (Brazil) and Ministerio de Ciencia, Tecnología e Innovación Productiva (Argentina). Funding has been provided by a University of York studentship and Old Dominion University research fellowship, additional support was provided by the NASA laboratory astrophysics

programme. The authors would like to thank the reviewer's for their comments during the review process and Daniel Frohman for identifying appropriate band strengths to use in calculation of the  $C_5$  and  $C_7$  column densities.

## REFERENCES

- Ádámkóvics M., Blake G. A., McCall B. J., 2003, *ApJ*, 595, 235  
 Agúndez M., Cernicharo J., 2006, *ApJ*, 650, 374  
 Agúndez M., Fonfría J. P., Cernicharo J., Kahane C., Daniel F., Guélin M., 2012, *A&A*, 543, A48  
 Bakker E. J., van Dishoeck E. F., Waters L. B. F. M., Schoenmaker T., 1997, *A&A*, 323, 469  
 Baronavski A. P., McDonald J. R., 1977, *J. Chem. Phys.*, 66, 3300  
 Bell M. B., Feldman P. A., Travers M. J., McCarthy M. C., Gottlieb C. A., Thaddeus P., 1997, *ApJ*, 483, L61  
 Bergeat J., Chevallier L., 2005, *A&A*, 429, 235  
 Bernath P. F., 2005, *Spectra of Atoms and Molecules*, 2nd edn. Oxford Univ. Press, Oxford  
 Bernath P. F., Hinkle K. H., Keady J. J., 1989, *Science*, 244, 562  
 Botschwina P., Sebald P., 1989, *Chem. Phys. Lett.*, 160, 485  
 Cami J., Bernard-Salas J., Peeters E., Malek S. E., 2010, *Science*, 329, 1180  
 Cernicharo J., Goicoechea J. R., Caux E., 2000, *ApJ*, 534, L199  
 Cernicharo J., Heras A. M., Tielens A. G. G. M., Pardo J. R., Herpin F., Guélin M., Waters L. B. F. M., 2001, *ApJ*, 546, L123  
 Cernicharo J. et al., 2010, *A&A*, 521, L8  
 Cernicharo J., Agúndez M., Guélin M., 2011, in Cernicharo J., Bachiller R., eds, *Proc. IAU Symp. 280, The Molecular Universe*. Cambridge Univ. Press, Cambridge, p. 237  
 Chen P. S., Yang X. H., 2012, *AJ*, 143, 36  
 Cherchneff I., 2006, *A&A*, 456, 1001  
 Cherchneff I., 2012, *A&A*, 545, A12  
 Cherchneff I., Glassgold A. E., 1993, *ApJ*, 419, L41  
 Crampton D., Cowley A. P., Humphreys R. M., 1975, *ApJ*, 198, L135  
 Cutri R. M. et al., 2003, *VizieR Online Data Catalog*, 2246, 0  
 Ducati J. R., 2002, *VizieR Online Data Catalog*, 2237, 0  
 Ehrenfreund P., Charnley S. B., 2000, *ARA&A*, 38, 427  
 Fischer H. et al., 2008, *Atmos. Chem. Phys.*, 8, 2151  
 Glassgold A. E., 1996, *ARA&A*, 34, 241  
 Goulay F., Nemes L., Schrader P. E., Michelsen H. A., 2010, *Mol. Phys.*, 108, 1013  
 Heath J. R., Saykally R. J., 1991, *J. Chem. Phys.*, 94, 1724  
 Herbst E., van Dishoeck E. F., 2009, *ARA&A*, 47, 427  
 Herzberg G., 1989, *Molecular Spectra and Molecular Structure: I. Spectra of Diatomic Molecules*. Krieger, Malabar, FL  
 Hinkle K. H., Bernath P. F., 1993, in Kwok S., ed., *ASP Conf. Ser. Vol. 41, Astronomical Infrared Spectroscopy: Future Observational Directions*. Astron. Soc. Pac., San Francisco, p. 125  
 Hinkle K. W., Keady J. J., Bernath P. F., 1988, *Science*, 241, 1319  
 Hinkle K. H., Cuberly R. W., Gaughan N. A., Heynssens J. B., Joyce R. R., Ridgeway S. T., Schmitt P., Simmons J. E., 1998, in Fowler A. M., ed., *Proc. SPIE Conf. Ser. Vol. 3354, Infrared Astronomical Instrumentation*. SPIE, Bellingham, p. 810  
 Jensen P., Rohlffing C. M., Almlöf J., 1992, *J. Chem. Phys.*, 97, 3399  
 Joyce R. R., 1992, in Howell S., ed., *ASP Conf. Ser. Vol. 23, Astronomical CCD Observing and Reduction Techniques*. Astron. Soc. Pac., San Francisco, p. 258  
 Kaiser R. I., 2002, *Chem. Rev.*, 102, 1309  
 Keady J. J., Hall D. N. B., Ridgeway S. T., 1988, *ApJ*, 326, 832  
 Keene J., Young K., Phillips T. G., Buettgenbach T. H., Carlstrom J. E., 1993, *ApJ*, 415, L131  
 Kranze R. H., Rittby C. M. L., Graham W. R. M., 1996, *J. Chem. Phys.*, 105, 5313  
 Krieg J. et al., 2013, *J. Phys. Chem. A*, 117, 3332  
 Li X., Millar T. J., Walsh C., Heays A. N., van Dishoeck E. F., 2014, *A&A*, 568, A111

- Loison J.-C., Wakelam V., Hickson K. M., Bergeat A., Mereau R., 2014, MNRAS, 437, 930
- McElroy D., Walsh C., Markwick A. J., Cordiner M. A., Smith K., Millar T. J., 2013, A&A, 550, A36
- Massó H., Veryazov V., Malmqvist P.-Å., Roos B. O., Senent M. L., 2007, J. Chem. Phys., 127, 154318
- Matsumura K., Kanamori H., Kawaguchi K., Hirota E., 1988, J. Chem. Phys., 89, 3491
- Menten K. M., Reid M. J., Kamiński T., Claussen M. J., 2012, A&A, 543, A73
- Menzies J. W., Feast M. W., Whitelock P. A., 2006, MNRAS, 369, 783
- Millar T. J., Herbst E., Bettens R. P. A., 2000, MNRAS, 316, 195
- Moazzen-Ahmadi N., McKellar A. R. W., 1993, J. Chem. Phys., 98, 7757
- Moazzen-Ahmadi N., McKellar A. R. W., Amano T., 1989, J. Chem. Phys., 91, 2140
- Mogren Al-Mogren M., Senent M. L., Hochlaf M., 2013, J. Chem. Phys., 139, 064301
- Mookerjee B. et al., 2012, A&A, 546, A75
- Neubauer-Guenther P., Giesen T. F., Schlemmer S., Yamada K. M. T., 2007, J. Chem. Phys., 127, 014313
- Olofsson H., 2008, Phys. Scr. T, 133, 014028
- Rothman L. S. et al., 2013, J. Quant. Spectrosc. Radiat. Transfer, 130, 4
- Seifahrt A., Käufel H. U., Zängl G., Bean J. L., Richter M. J., Siebenmorgen R., 2010, A&A, 524, A11
- Souza S. P., Lutz B. L., 1977, ApJ, 216, L49
- Špirko V., Mengel M., Jensen P., 1997, J. Mol. Spectrosc., 183, 129
- Tsuji T., 1973, A&A, 23, 411
- Vala M., Chandrasekhar T. M., Szczepanski J., van Zee R., Weltner W., Jr, 1989, J. Chem. Phys., 90, 595
- Whitelock P. A., Feast M. W., Marang F., Groenewegen M. A. T., 2006, MNRAS, 369, 751
- Zhang Y., Kwok S., Dinh-V-Trung, 2009a, ApJ, 691, 1660
- Zhang Y., Kwok S., Nakashima J.-i., 2009b, ApJ, 700, 1262
- Ziurys L. M., 2006, Proc. Natl. Acad. Sci., 103, 12274

This paper has been typeset from a  $\text{\TeX}/\text{\LaTeX}$  file prepared by the author.